García García, D.; Rayón Encinas, E.; Carbonell Verdú, A.; López-Martínez, J.; Balart Gimeno, RA. (2017). Improvement of the compatibility between poly(3-hydroxybutyrate) and poly(e-caprolactone) by reactive extrusion with dicumyl peroxide. European Polymer Journal. 86:41-57. doi:10.1016/j.eurpolymj.2016.11.018.

“Improvement of the compatibility between poly(3-hydroxybutyrate) and poly(ε-caprolactone) by reactive extrusion with dicumyl peroxide”

D. Garcia-Garcia*, E. Rayón, A. Carbonell-Verdu, J. Lopez-Martinez, R. Balart.

Instituto de Tecnología de Materiales-ITM

Universitat Politècnica de València

Plaza Ferrandiz y Carbonell 1, 03801, Alcoy, Alicante (Spain)

* Corresponding author: D. Garcia-Garcia

E-mail: dagarga4@epsa.upv.es

Tel.: (+34) 96 652 84 34

Fax: (+34) 96 652 84 33

ABSTRACT

Poly(3-hydroxybutyrate) is a biodegradable aliphatic polyester obtained through bacterial fermentation that has gained attention in the last few years; nevertheless, its industrial applications are restricted because of some drawbacks related to its high stiffness and fragility which is associated to its high crystallinity. In this work, poly(3-hydroxybutyrate) (P3HB) was melt blended with poly(ε-caprolactone) (PCL) at a constant weight ratio of 75/25 (P3HB/PCL) by reactive extrusion with different contents of dicumyl peroxide (DCP) in the 0 – 1 wt% range. The effects of the DCP load on mechanical, thermal and morphology of the P3HB/PCL blend were studied. Results showed a positive increase in the elongation at break and the impact-absorbed energy of 91% and 231% respectively with regard the uncompatibilized P3HB/PCL blend by the addition of 1 wt% DCP, being this a clear evidenced of the improved compatibility between these polymers. Moreover, morphology of DCP-compatibilized P3HB/PCL blend obtained by field emission electron microscopy (FESEM) and atomic force microscopy (AFM) showed a remarkable decrease in the particle size of poly(ε-caprolactone)-rich domains randomly dispersed in the poly(3-hydroxybutyrate). In addition, both FESEM and AFM also revealed improved interfacial adhesion between P3HB- and PCL-rich phases with a noticeable decrease in the gap between them. Addition of 1 wt% DCP also contributes to lowering the degree of crystallinity of PHB by 14% in the blend and other thermal properties are not highly affected by the reactive extrusion with DCP.

Keywords: Poly(3-hydroxybutyrate); poly(ε-caprolactone); dicumyl peroxide; reactive compatibilization; blends.

INTRODUCTION

During the last years, a global marked driven by consumerism along with the relatively low price of plastic materials has led to a remarkable growth in the plastic production and consumption. Only in Europe the plastic production in 2014 was estimated to 59 million tons whilst the global plastic production was of about 299 million tons. The packaging industry is the biggest consumer which accounts for 39.5% with a wide variety of products characterized by a very short life cycle [1]. One of the main problems related to the massive use of plastics is the huge amounts of wastes that are generated after the end of their life cycled as only a small amount is recycled, upgraded or incinerated for energy production. The most common situation is that huge amounts of plastic wastes are continuously deposited into controlled landfills with a marked negative effect on environment. It has been estimated that in 2014 the total amount of plastic wastes poured into European's landfills accounts to 8 million tons [1]. The use of biodegradable plastics is an environmentally friendly solution to the abovementioned problems. There is a wide variety of biodegradable plastics that are compostable in certain conditions. Among this, it is possible to find biodegradable polymers from both petroleum and renewable resources. Nevertheless, most of them are currently expensive and this restricts their use at industrial scale. On the other hand, biodegradable plastics have to face an important technical challenge as currently, most of them offer inferior properties to conventional commodity and engineering plastics from petroleum origin [2]. During the last years, a remarkable increase in the research and development of industrial formulations based on biodegradable plastics has been detected with the main aim of obtaining a set of environmentally friendly materials that are capable to compete with conventional petroleum-derived plastics in terms of technical features and costs [3].

Código de campo cambiado

Código de campo cambiado

Código de campo cambiado

Código de campo cambiado

Poly(3-hydroxybutyrate) (P3HB) is one of the most promising biopolymers. It is an aliphatic polyester that is synthesized through bacterial fermentation and it is characterized by its biocompatibility and biodegradability [4]. Despite these interesting features, P3HB polymer chains are highly stereoregular and this gives highly crystalline polymers (with a degree of crystallinity over 55%). On the other hand, as its glass transition temperature (T_g) is located

Código de campo cambiado

below the room temperature (typically around 0-2 ºC), P3HB undergoes physical aging related to secondary crystallization [5, 6]. For this reason, P3HB is a highly fragile polymer with very low plastic deformation [7]. Another important drawback is its relatively narrow processing window in terms of temperature as it degradation occurs close to its melting [8]. All these technical drawbacks, together with its high price compared to conventional commodity plastics, restrict its use at industrial scale [9].

There have been many attempts to overcome the intrinsic fragility of P3HB polymers by different approaches: internal copolymerization with other flexible monomers [10-12], external plasticization [13-15] or melt blending with different polymers and/or copolymers [16-19]. External mixing of P3HB with several polymers is an effective method, from both technical and economical points of view, to overcome all the abovementioned drawbacks. In a previous work [20], P3HB was melt blended with poly(ε-caprolactone) (PCL) and as per the results, P3HB/PCL blends with 25 wt% PCL led to materials with improved toughness with a slight increase in both elongation at break and impact-absorbed energy by 38% and 30% respectively. Nevertheless, P3HB and PCL polymers are immiscible (or very low miscible) polymers and phase separation occurs when melt-blended leading to a typical droplet structure with a PH3B-rich matrix phase in which PCL-rich domains are embedded [21]. For this reason, compatibilization of P3HB/PCL blends is a critical issue to be addressed as the overall mechanical properties of a multiphase system are directly related to the ability of its components to transfer stresses [22]. One interesting method to improve compatibility is by reactive extrusion during compounding; this method is technologically preferable to addition of tailored copolymers [23]. Reactive extrusion is a simple and cost effective technique for polymer processing. In this, the extruder plays the role of a continuous chemical reactor in which, two different operations occur simultaneously. Melt extrusion and chemical reaction (polymer synthesis and/or modification or in situ compatibilization of polymer blends) are carried out in just one stage [24, 25]. Reactive extrusion offers some advantages such as it is not necessary to use solvents, allows a full control of the residence times, it is an online process and the technical equipment and accessories are relatively cheap [25, 26]. Dicumyl peroxide (DCP) is a free

Código de campo cambiado
Código de campo cambiado
Código de campo cambiado
Código de campo cambiado
Código de campo cambiado
Código de campo cambiado
Código de campo cambiado
Código de campo cambiado
Código de campo cambiado
Código de campo cambiado
Código de campo cambiado

radical initiator widely used in polymerization processes, natural rubber vulcanization and as crosslinker [23]. It has been used to promote compatibilization of immiscible polymers in different binary blends. W. Dong *et al*. [27] observed an increase in tensile strength of 5 MPa and a remarkable improvement of the energy absorption of about 30% by the only addition of 0.5 wt% DCP to binary blends of PHB and PDLLA (70/30). They also reported a noticeable decrease in the PDLLA domain size dispersed in the PHB matrix which is representative for somewhat partial reticulation between these two polymers. P. Ma *et al.* [21] also observed an increase in the elongation at break and the impact-absorbed energy after addition of 0.5 wt% DCP in a PHB/PBS (70/30) blend with regard to the same uncompatibilized system. In fact, the elongation at break changed from 2% to 11% and the impact-absorbed energy increased from 9 kJ m^{-2} to 54 kJ m^{-2}.

Código de campo cambiado

The present work is focused on the evaluation of the effects of DCP on final performance of binary blends from poly(3-hydroxybutyrate) (P3HB) and poly(ε-caprolactone) (PCL) processed by *in situ* reactive compatibilization extrusion. The effects of different DCP loads (0, 0.25, 0.50, 0.75 and 1 wt%) is evaluated in terms of mechanical and thermal properties of the P3HB/PCL (75/25) blend as well as its morphology.

EXPERIMENTAL

Materials

Poly(3-hydroxybutyrate) P3HB pellets (P226, M_w = 426,000 Da) were supplied by Biomer (Krailling, Germany). Poly(ε-caprolactone) (PCL) (CAPA 6500, M_w = 50,000 Da) was provided by Perstorp Holding AB (Malmö, Sweden). Dicumyl peroxide (DCP) (98% purity) was supplied from Sigma Aldrich (Madrid, Spain).

Sample processing

P3HB and PCL were dried in a vacuum oven at 70 ºC and 40 ºC for 24 h respectively to remove residual moisture. P3HB/PCL (75/25) blends with different DCP (0, 0.25, 0.50, 0.75 and 1 wt%) were melt-blended in a twin-screw co-rotating extruder (L/D= 24, D= 25 mm) from

DUPRA S.L. (Castalla, Spain) at a rotating speed of 40 rpm. Under these conditions, the residence time for the *in situ* compatibilization of P3HB/PCL blends by reactive extrusion process was about 55 s. The temperature profile of the extrusion barrel was set to 165 ºC (hopper), 170 ºC, 175 ºC and 180 ºC (die). Before the *in situ* compatibilization extrusion process, all three components (P3HB, PCL and DCP) were mechanically mixed in a zipper bag to obtain homogeneous pre-mixing. After extrusion, the material was cooled to room temperature and subsequently, it was pelletized. Standard samples for tensile, flexural and impact tests were obtained by injection moulding in a Meteor 270/75 from Mateu & Solé (Barcelona, Spain) with a temperature profile of 165 ºC, 165 ºC, 170 ºC, 175 ºC and 180 ºC from the hopper to the injection nozzle. Table 1 summarizes the compositions and labelling of the different formulations.

Table 1. Composition and labelling of binary poly(3-hydroxybutyrate) (P3HB) and poly(ε-caprolactone) (PCL) blends *in situ* compatibilized by reactive extrusion with different amounts of dicumyl peroxide (DCP).

Coding	**P3HB (wt%)**	**PCL (wt%)**	**DCP (wt%)**
PHB	100	0	0
PHB/PCL	75	25	0
PHB/PCL/DCP/25	75	25	0.25
PHB/PCL/DCP/50	75	25	0.50
PHB/PCL/DCP/75	75	25	0.75
PHB/PCL/DCP/100	75	25	1

Characterization techniques

Gel fraction

The gel fraction of the P3HB/PCL blends *in situ* compatibilized with different DCP amount was determined by soxhlet extraction in boiling chloroform for 72 h. The extracted

samples were dried in an air circulating oven at 40 ºC until a constant weight was obtained. The gel fraction was calculated using the following equation (1):

$$gel\ fraction\ (wt\%) = \frac{m_1}{m_0} \times 100 \qquad \text{Eq.1}$$

Where m_0 and m_1 represent the weight of the dry samples before and after the extraction process, respectively.

Mechanical properties

The glass transition temperature of P3HB is located below room temperature, typically in the 0-2 ºC range. When P3HB is stored at room temperature, secondary crystallization occurs which has a marked effect on physical aging as it has been reported [28]. This process causes a remarkable decrease in the elongation at break while the elastic modulus and tensile strength are not highly affected. The most important changes take place in the first two weeks and tend to stabilize at an aging time of 21 days. For this reason, mechanical properties of the P3HB/PCL blend compatibilized with different DCP loads were obtained by standard tensile, flexural an impact tests after 22 days of the injection moulding.

Código de campo cambiado

Tensile and flexural properties were obtained according to ISO 527 and ISO 178 standards respectively, using a universal test machine Ibertest ELIB 30 from SAE Ibertest (Madrid, Spain) at room temperature. Both tests were carried out with a 5 kN load cell and a crosshead speed of 5 mm min^{-1}. At least five different specimens were tested and average values of the main mechanical parameters were calculated. In addition, the elastic modulus was accurately determined using an axial extensometer IB/MFQ-R2 from Ibertest (Madrid, Spain) coupled to the universal test machine.

A 1 J Charpy impact pendulum from Metrotec SA (San Sebastian, Spain) was used to obtain the impact-absorbed energy of the P3HB/PCL blend compatibilized with different DCP loads. Standard notched samples (“V” notch type at 45º with a notch radius of 0.25 mm) were

tested following the guidelines of the ISO 179 international standard. The values of the impact-absorbed energy were calculated as the average of the energies obtained for five different samples.

Thermal properties

Thermal degradation at elevated temperatures of P3HB/PCL blend compatibilized with different DCP loads was analysed by thermogravimetry (TGA) in a TGA/SDT 851 thermobalance from Mettler-Toledo Inc. (Schwerzenbach, Switzerland) Samples with an average size ranging from 7 to 9 mg were placed in standard alumina pans and were subjected to a heating program from 30 ºC up to 600 ºC at a constant heating rate of 10 ºC min^{-1} under nitrogen atmosphere with a flow rate of 66 mL min^{-1}. The onset degradation temperature (T_0) was determined as the temperature corresponding to a weight loss of 5% and the maximum degradation rate temperature for each stage was obtained as the corresponding peak in the derivative TGA curve (DTG).

Differential scanning calorimetry (DSC) experiments were carried out in a DSC Mettler-Toledo 821 calorimeter from Mettler-Toledo Inc. (Schwerzenbach, Switzerland). The heating and cooling rates for the all the scans were set to 10 ºC min^{-1} under nitrogen atmosphere (flow rate 66 mL min^{-1}). 7-10 mg of the corresponding material were placed in standard 40 µL aluminium pans. The thermal program consisted on a first heating cycle from -50 ºC to 180 ºC, a second stage consisting on an isothermal cycle at 180 ºC for 2 min. Then a cooling process down to -50 ºC was applied and, finally, a heating cycle up to 300 ºC was applied. The melting temperature (T_m) was obtained from the second heating cycle and the degree of crystallinity of P3HB ($X_{c,\,P3HB}$) and PCL ($X_{c,\,PCL}$) was calculated by the following equation:

$$X_c\,(\%) = 100 \times \left[\frac{\Delta H_m}{\Delta H_0 \cdot w}\right] \qquad \text{Eq. 2}$$

Where ΔH_m is the thermodynamic melt enthalpy per gram, ΔH_0 is the theoretical melt enthalpy associated to the corresponding 100% crystalline polymer (these values were assumed to be 146 J g^{-1} [29] for P3HB and 156.8 J g^{-1} [30] for PCL), and *w* is the weight fraction of the corresponding polymer (P3HB or PCL) in the blend.

Código de campo cambiado

Dynamic Mechanical Analysis (DMA)

The evolution of the storage modulus (G') and the damping factor (tan δ) of P3HB/PCL blend compatibilized with different DCP loads as a function of temperature was obtained by an oscillatory rheometer AR GS from TA Instruments (New Castle, USA) equipped with a special clamp system for solid samples. Samples with a size of 40x10x4 mm^3 were subjected to a temperature program from -100 ºC up to 100 ºC at a constant heating rate of 2 ºC min^{-1}, a frequency of 1 Hz and a maximum shear strain (γ) of 0.1%. The glass transition temperature (T_g) was assumed as the peak maximum of the damping factor curve.

Field emission scanning electron microscopy (FESEM)

Fractured surfaces from impact tests were coated with a thin layer of platinum in a high vacuum sputter coater EM MED20 from Leica Microsystem (Milton Keynes, United Kingdom) prior to be observed the phase morphology in a field emission scanning electron microscopy (FESEM) ZEISS ULTRA55 (Oxford instruments) operated at a voltage of 2 kV. Micrographs were registered at 2500x and 10000x magnification.

Atomic Force Microscopy (AFM) and Peak Force QNM

Young´s modulus of each individual phase in the P3HB/PCL and P3HB/PCL compatibilized with 1 wt% DCP blends was obtained using an atomic force microscope, AFM model Nanoscop II from Veeco National Instrument (Santa Barbara, California, USA) working in peak force tapping mode by the quantitative nanomechanical measurement, QNM method [31, 32]. With this analysis the height map, deformation and adhesion of each area was obtained. By using this method it is possible the acquisition of force-penetration curves by

Código de campo cambiado

Código de campo cambiado

indenting the material, at a high speed (2 kHz) under very low penetration depths [33, 34]. By using these indentation curves, the software generates different image maps with z-heights, elastic modulus (E), adhesion and elastic deformation. The Derjaguin-Muller-Toporov (DMT) model was selected to calculate the elastic modulus as it has given good results for soft materials, nanocomposites, fibrils, live cells and very thin layers from the data provided by instrumented indentation techniques [35-39]. The DMT model alloys calculation of the elastic modulus by analysing the unload stage using the following expression [40].

Código de campo cambiado

Código de campo cambiado

$$F_{tip} = F - F_{adh} = \frac{4}{3} E_r \sqrt{R(d - d_0)^3} \qquad \text{Eq. 3}$$

Where $F\text{-}F_{adh}$ is the force on the cantilever relative to the adhesion force, R is the tip radius, and $d\text{-}d_0$ is the deformation of the sample. In this study, the region comprised between 10% and 70% of the unload curve was fitted by DMT model calculations. The contact radius, R, was determined for a fixed working z-displacement of 5-10 nm. Calibration was carried out by the relative calibration method which uses a sample of known modulus to obtain the ratio of the spring constant to the square root of the tip end radius. In this study a polystyrene (PS) pattern with a nominal elastic modulus, E, of 2.7 GPa was used as the reference material and the obtained $R_{5\text{-}10\ nm}$ value was 9 nm. Calibration of the tip radius was done before and after finishing the study to guarantee negligible changes due to wear. The spring constant was calibrated, reporting a stiffness of 5 N m^{-1}. The applied force during the scanning was the required to keep a contact depth in the 5-10 nm range. The scan frequency was 0.75 Hz, 0.5 Hz and 0.3 Hz on squared areas sizing 3x3 μm^2, 10x10 μm^2 and 20x20 μm^2. All tests were conducted on 500 µm thick films obtained by environmental ultramicrotomy.

Nanomechanical properties

Nanoindentation tests were carried out in a Nanoindenter G-200 from Agilent Nanotechnology (Santa Clara, California, USA). A Berkovich tip was calibrated with Pyrex as

reference material. An array of 75 indentations with a depth of 150 nm with a separation of 3 μm between them was programmed. Calculation of the stiffness was done by using the Continuous Stiffness Measurement method [41] with an oscillation of 2 nm at a frequency of 70 Hz. Calculation of hardness (H) and the elastic modulus (E) was done using the Oliver&Pharr method [42] by averaging the values in a depth range between 100 and 150 nm. All the depth values were corrected by taking into account the adjustment proposed by Loubet [43, 44] for polymeric materials with adhesive contact and assuming a Poisson ratio, υ, of 0.3 to calculate the elastic modulus, E.

Código de campo cambiado

RESULTS AND DISCUSSION

Gel fraction of P3HB/PCL blends compatibilized by reactive extrusion with DCP

Fig. 1 shows the plot evolution of the gel fraction with increasing DCP content during the *in situ* compatibilization by reactive extrusion of P3HB and PCL blends. As it can be seen, the gel content increases with the DCP content with a maximum of 18.8% for a DCP content of 1 wt%. DCP decomposes and acts as a free radical initiator. These free radicals promote the formation of P3HB and PCL macroradicals by hydrogen abstraction. Then, the combination of these macroradicals leads to formation of P3HB-co-PCL copolymers that positively contribute to compatibilization and formation of partially crosslinked networks in the blends. Nevertheless, not only P3HB and PCL reactions occur but also PCL-rich domains can establish stronger interactions with the P3HB polymer matrix. Hence, the use of DCP during the reactive extrusion process gives a series of products such as grafted/branched/crosslinked P3HB and PCL chains, P3HB-co-PCL copolymers and partially crosslinked P3HB/PCL networks [21, 45]. Furthermore, the melting process also promotes chain scission due to the high thermal instability of P3HB together with the high thermal stability of the free radicals, thus leading to formation of more complex products. These reactions can be observed in **Fig. 2**. [46, 47].

Código de campo cambiado

Código de campo cambiado

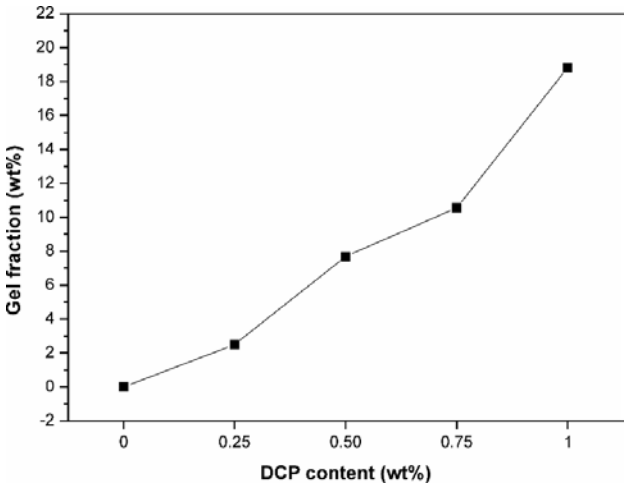

Figure 1. Plot evolution of the gel fraction obtained by soxhlet extraction of the P3HB/PCL (75/25) blend as a function of DCP content used for reactive extrusion

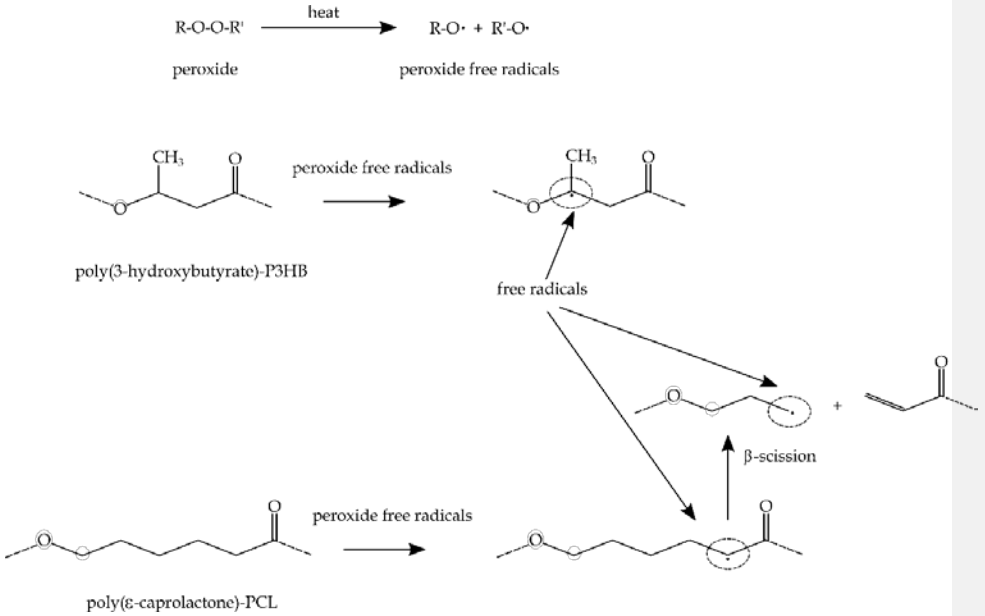

Figure 2. Schematic representation of free radical formation on poly(3-hydroxybutyrate) and poly(ε-caprolactone) polymer chains by reaction with peroxide free radicals

Mechanical properties of P3HB/PCL blends compatibilized by reactive extrusion with DCP

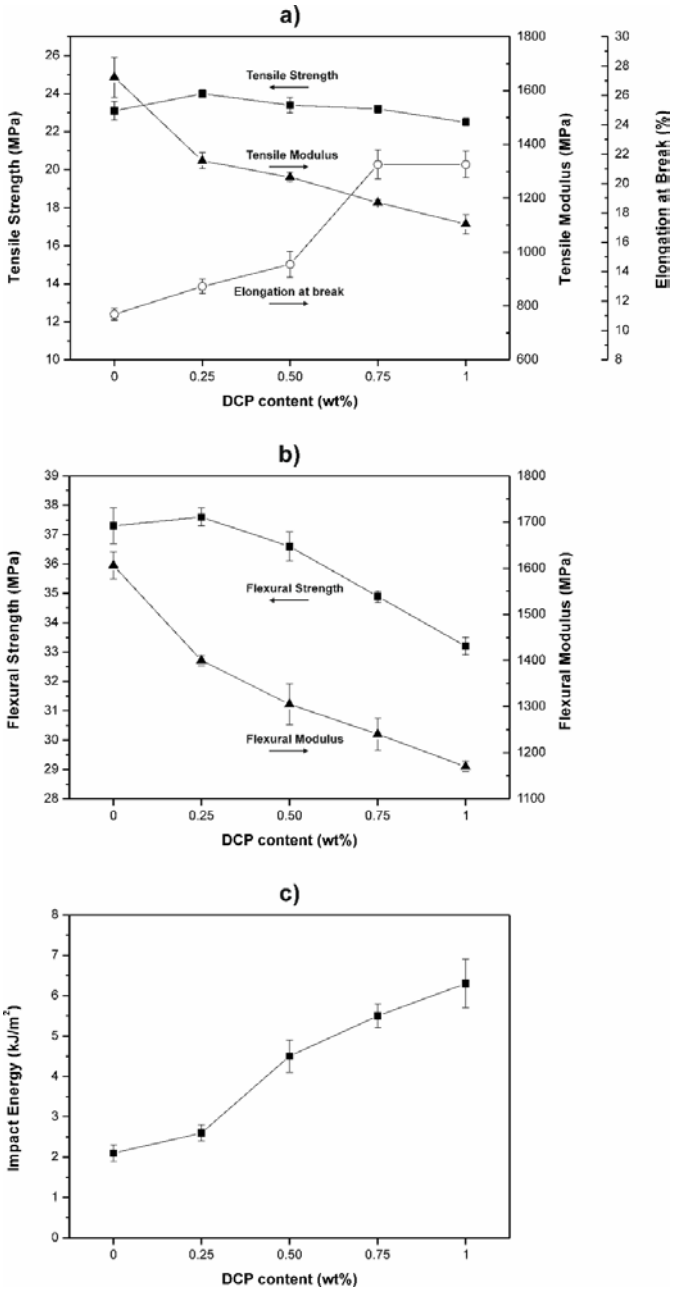

Figure 3. Mechanical properties of the P3HB/PCL (75/25) blend as a function of DCP content used for reactive extrusion: a) tensile properties, b) flexural properties and c) impact properties

The only addition of 25 wt% PCL to P3HB leads improved toughness. These uncompatibilized blends, are characterized by a droplet structure in which, PCL-rich domains a finely dispersed into the P3HB matrix. Although a slight increase in ductile properties are achieved, this improvement is not so high as we report in a previous work [20]. **Fig. 3** gathers the main results corresponding to mechanical characterization of P3HB/PCL (75/25) blends with different DCP used for the reactive extrusion process. With regard to tensile properties, it is clear to see that the only addition of 0.25 wt% DCP during the reactive extrusion leads to increased compatibility. In fact, the tensile strength is slightly increased from 23.1 MPa (uncompatibilized P3HB/PCL) up to 24 MPa. DCP content over 0.25 wt% leads to slightly lower tensile strength values of 22.5 MPa for the compatibilized blend with 1 wt% DCP. So that, it is worthy to note that reactive extrusion with different DCP loads does not affect in a noticeable way to tensile strength. On the other hand, the elongation at break is remarkably improved as the DCP load for reactive extrusion increases. As it can be seen in **Fig. 3a**, uncompatibilized P3HB/PCL (75/25) blend is characterized by a relatively low elongation at break value of 11.1%. In fact, the elongation at break for compatibilized P3HB/PCL blend with 0.75 wt% DCP and 1.0 wt% DCP changes up to values close to 21.3% which represents a percentage increase of almost 91%, thus giving clear evidences of improved ductile properties after the reactive extrusion. This could be related to improved interactions between the P3HB-rich phase and the PCL-rich phase. Regarding the tensile modulus, as it is defined as the ratio of stress to elongation in the linear region, it is expectable a decrease. As it has been stated previously, the tensile strength does not change in a noticeable way whilst the elongation at break increases in a remarkable way. For this reason, the ratio stress to elongation decreases. In fact, the tensile modulus changes from 1649 MPa (uncompatibilized P3HB/PCL blend) down to

Código de campo cambiado

1104 MPa for the blend compatibilized with 1 wt% DCP during the reactive extrusion process which represents a percentage decrease of about 33%.

Similar tendency can be observed for flexural properties. The flexural strength remains almost constant at values of 37 MPa for DCP content in the 0-0.25 wt% range while a slight decrease is detected over 0.25 wt% DCP with minimum values of 33.2 MPa for the P3HB/PCL blend compatibilized with 1 wt% DCP during the reactive extrusion. The flexural modulus offers identical tendency as that observed for the tensile modulus with a decrease from 1606 MPa for the uncompatibilized blend down to 1170 MPa for the blend compatibilized by reactive extrusion with 1 wt% DCP.

The impact-absorbed energy is, as other ductile properties in a polymer blend such as the elongation at break, highly sensitive to compatibility between components as it is related to material cohesion and the typical droplet structure of an immiscible blend negatively contributes to cohesion. **Fig. 3c** shows the evolution of the impact-absorbed energy with increasing DCP content during the reactive extrusion. It is worthy to note the remarkable increase in the impact-absorbed energy from values of about 2 kJ m^{-2} (uncompatibilized blend) up to values of 6.3 kJ m^{-2} that represents a percentage increase of 231%. This noticeable increase indicates a clear improvement of the cohesion and this indicates that interactions between P3HB-rich phase and PCL-rich phase have improved as a consequence of the use of the peroxide as *in situ* compatibilizer by reactive extrusion. In the case of the uncompatibilized P3HB/PCL (75/25) blend, the lack of interactions between both polymers promotes phase separation and this leads to interface failure when an external stress is applied; then, microcrack formation and subsequent growth is very fast and this has a negative effect on the total impact-absorbed energy with a pronounced fragile behaviour. Reactive extrusion with DCP increases interactions between the P3HB-rich phase and the PCL-rich phase and this has a positive effect on load transfer due to improved phase-continuity. Hence, it is possible to conclude that reactive extrusion with DCP has a positive effect on compatibilizing P3HB and PCL in their blends with a remarkable improvement of ductile properties such as elongation at break and impact-absorbed energy due to increased material cohesion.

Thermal properties of P3HB/PCL blends compatibilized by reactive extrusion with DCP

DSC curves of the second heating cycle of P3HB/PCL (75/25) blend are shown in **Fig. 4** and the main thermal parameters obtained from DSC analysis are summarized in Table 2. As it can be seen the DSC thermogram of neat P3HB shows a main melting peak at 174.8 ºC and a small melt peak located at 52.3 ºC which could be related to the melting of some low molecular weight additive contained in the commercial formulation [48]. As expected, uncompatibilized P3HB/PCL (75/25) blend offers two clear melt processes located at 172.9 ºC and 56.3 ºC that correspond to the melting of P3HB and PCL individual polymers respectively. Compatibilization by reactive extrusion with DCP leads to some changes in the thermal behaviour of the blend. As it can be seen, the peak size of PCL is smaller as the DCP content in the reactive extrusion process increases. This fact suggests a conversion of the PCL-rich domains into amorphous as the DCP content increases. On the other hand, DCP does not affect the melting temperature of PCL but it is worthy to note a slight decrease in the P3HB melting temperature by almost 4 ºC with regard to the uncompatibilized blend. Regarding the degree of crystallinity of both P3HB and PCL in the P3HB/PCL (75/25) blend, values of 39.8% and 45.7%, respectively, are obtained. The use of 0.25 wt% and 0.50 wt% DCP during the reactive extrusion process does not affect in a noticeable way to the crystallinity of both P3HB- and PCL-rich domains. Over 0.50 wt% DCP it is possible to observe a slight decrease in the overall crystallinity of both polymers in the blend. This fact also explains why both tensile and flexural moduli are lower with increasing DCP content during the reactive extrusion.

Código de campo cambiado

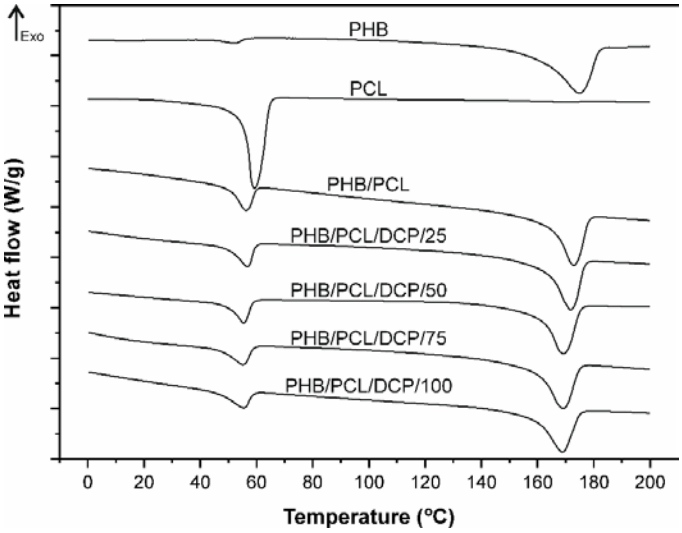

Figure 4. DSC curves of the second heating cycle of neat P3HB, neat PCL, uncompatibilized P3HB/PCL (75/25) blend and compatibilized blend by reactive extrusion with different DCP content

The main thermal parameters corresponding to the thermal degradation of P3HB/PCL (75/25) blend are summarized in Table 2. Thermal degradation of neat P3HB occurs in two separated stages which is directly related to the complex chemical composition of the commercial formulation with plasticizers, nucleating agents, fillers and stabilizers [48]. Uncompatibilized P3HB/PCL (75/25) blend also shows two degradation stages. The first one is characterized by a maximum degradation rate temperature of 302.3 ºC and is assigned to P3HB whilst the second one, at higher temperatures of 422.3 ºC corresponds to the maximum degradation rate temperature of PCL as this is more stable than P3HB to thermal degradation. Regarding the onset degradation temperature (T_0) it is possible to observe that, in general, PCL has a positive effect on thermal stabilization with an increase from 246.7 ºC for neat P3HB up to 282.7 ºC for its blend with 25 wt% PCL (uncompatibilized). The obtained data indicate that no significant change in the onset degradation temperature is obtained by reactive extrusion with

Código de campo cambiado

different DCP loads as T_0 ranges from 280 ºC to 285 ºC for all DCP contents used in the reactive extrusion process.

Table 2. Thermal parameters of neat P3HB, neat PCL, uncompatibilized P3HB/PCL (75/25) blend and P3HB/PCL (75/25) blends compatibilized by reactive extrusion with different DCP contents

Samples	DSC Parameters						TGA Parameters		
	$T_{m\ PCL}$ (ºC)	$\Delta H_{m\ PCL}$ (J g^{-1})	$X_{c\ PCL}$ (%)	$T_{m\ PHB}$ (ºC)	$\Delta H_{m\ PHB}$ (J g^{-1}]	$X_{c\ PHB}$ (%)	T_0 (ºC)[a]	$T_{max\ PHB}$ (ºC)	$T_{max\ PCL}$ (ºC)
PHB	-	-	-	174.8	-75.8	51.9	246.7	272.3	382.0
PCL	60.0	-72.8	46.4	-	-	-	379.5	-	415.8
PHB/PCL	56.3	-62.5	39.8	172.9	-66.8	45.7	282.7	302.3	422.3
PHB/PCL/DCP/25	56.7	-61.2	39.0	171.7	-66.8	45.7	283.6	302.3	422.3
PHB/PCL/DCP/50	55.5	-58.4	37.4	169.2	-66.3	45.4	285.4	302.3	422.3
PHB/PCL/DCP/75	55.2	-54.8	35.0	169.1	-60.5	41.4	282.6	302.3	422.3
PHB/PCL/DCP/100	55.5	-49.0	31.3	168.8	-57.3	39.3	279.0	302.3	422.3

[a] T_0, calculated at 5% mass loss.

Dynamic mechanical thermal analysis (DMTA) of P3HB/PCL blends compatibilized by reactive extrusion with DCP

Fig. 5 shows the plot evolution of the damping factor (tan δ) and the storage modulus (G') of uncompatibilized P3HB/PCL (75/25) blend and the same blend composition compatibilized with different DCP content by reactive extrusion. The glass transition temperature (T_g) was obtained through the peak maximum in the damping factor curves. As one can see, two different relaxation processes are present which are attributed to immiscibility between P3HB and PCL. Reactive extrusion with DCP leads to partially compatibilized blends with a slight increase in the T_g of the PCL-rich domains from -68.3 ºC (uncompatibilized blend) up to -65 ºC for the blend compatibilized by reactive extrusion with 0.75 wt% and 1 wt% DCP. This slight increase can be attributed to a restriction of the PCL segments movement along the

interphase with increased miscibility [21]. On the other hand, the glass transition temperature of the P3HB-rich domains does not change in a significant way and remains at values around 1 ºC. By observing the evolution of the storage modulus (G') in **Fig. 5b** it can be clearly seen a decrease of G' for all blends compatibilized with different DCP contents. At low temperatures (below the $T_{g,\ PCL}$), all blends show high storage modulus values (more than 2000 MPa) due to high rigidity of the polymeric chains. After reactive extrusion with DCP, a slight decrease in G' can be observed as the DCP content increases. In fact, the lowest G' values are obtained for the blend compatibilized by reactive extrusion with 1 wt% DCP. The effects of this *in situ* compatibilization by reactive extrusion are more evident in the rubbery state comprised between the glass transition of both neat polymers, -53 ºC for PCL and 1 ºC for P3HB [20]; this is due to the fact that in situ compatibilization affects the overall movement of the molecular chain segments instead of the localized macromolecule movements [45]. This decrease is due to increased compatibility which is achieved by anchoring poly(ε-caprolactone) macroradicals (promoted by DCP at elevated temperatures) to poly(3-hydroxybutyrate) macroradicals. In addition, P3HB-P3HB, PCL-PCL and P3HB-PCL crosslinking can also occur as a consequence of the radicals formed by DCP.

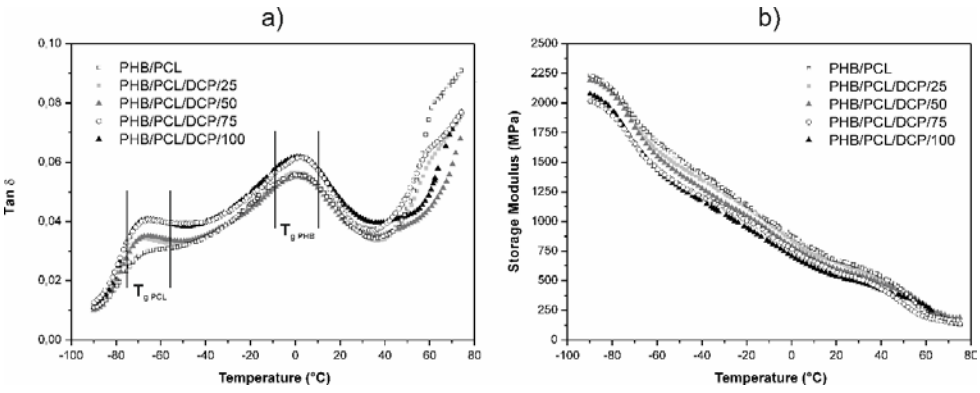

Figure 5. Dynamic mechanical thermal analysis (DMTA) of uncompatibilized P3HB/PCL (75/25) blend and compatibilized blends by reactive extrusion with different DCP contents as a function of temperature: a) damping factor, tan δ and b) storage modulus, G'

Morphology study of P3HB/PCL blends compatibilized by reactive extrusion with DCP

Fig. 6 shows the morphology of fractured surfaces from impact tests without compatibilization and with compatibilization by reactive extrusion with different DCP content. As it can be observed, uncompatibilized P3HB/PCL (75/25) blend (**Fig. 6a** and **Fig. 6b**) shows a clear phase separation with a typical droplet structure indicating immiscibility. The PCL-rich domains appear as randomly dispersed droplets with a particle size comprised in a wide range into the P3HB polymer matrix. In addition, small gaps can be detected along PCL-rich and P3HB-rich domains thus evidencing poor interfacial adhesion between these two polymers as stated by D. Garcia-Garcia *et al.* [20]. It is also detectable some plastic deformation of PCL-rich domains during the impact test. The reactive extrusion with DCP has a remarkable effect on the morphology of the P3HB/PCL (75/25) blend as it can be seen in **Fig. 6c** to **Fig. 6f**. As it can be seen, the gaps between the PCL- and P3HB-rich domains have almost disappeared and the interface between them is not detectable. The use of DCP as reactive compatibilizer leads to a decrease in size on PCL-rich domains leading to a high homogeneous fracture surface without the typical filament formation on PCL-rich domains. All these features are indicating that the reactive extrusion with DCP has a positive effect on improving the miscibility of P3HB and PCL polymers with the subsequent improvement on mechanical ductile properties as described before.

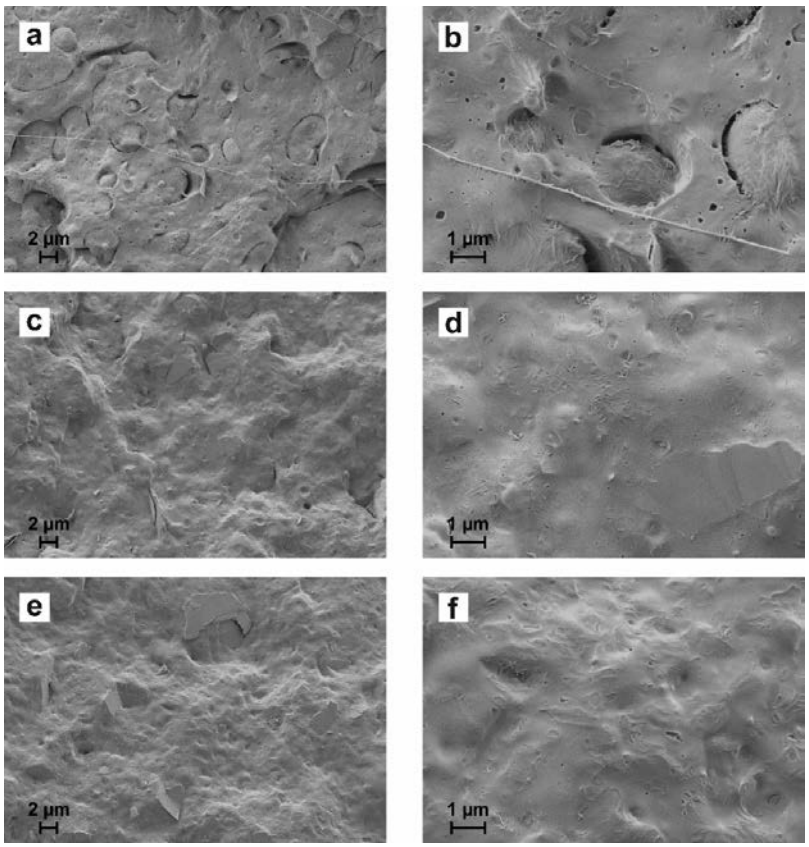

Figure 6. FESEM images of impact-fractured surfaces of: (a) uncompatibilized P3HB/PCL (75/25) at 2500x; (b) uncompatibilized P3HB/PCL at 5000x; (c) P3HB/PCL (75/25) compatibilized by reactive extrusion with 0.50 wt% DCP at 2500x; (d) P3HB/PCL (75/25) compatibilized by reactive extrusion with 0.50 wt% DCP at 5000x; (e) P3HB/PCL (75/25) compatibilized by reactive extrusion with 1 wt% DCP at 2500x and (f) P3HB/PCL (75/25) compatibilized by reactive extrusion with 1 wt% DCP at 5000x

Atomic Force Microscopy (AFM) and PeakForce QNM

An in-depth study of the effect of DCP on the microstructure of P3HB/PCL blends was carried using atomic force microscopy (AFM) working in the Quantitative Nanomechanical PeakForce, QNM mode. This method allows obtaining an image map not only of deformations and z-displacements but also of the elastic and adhesive properties of the analysed surface.

Ultramicrotome samples of P3HB/PCL and P3HB/PCL compatibilized with 1 wt% DCP were analysed by the AFM technique. Some attempts did not give useful image maps due to the high roughness of fractured samples as reported by other authors [49].

Fig. 7 shows the image maps of the abovementioned P3HB/PCL systems (uncompatibilized and compatibilized system by reactive extrusion with 1 wt% DCP) under different AFM channels. **Fig. 7a** shows the topographic AFM image (height channel) of the uncompatibilized P3HB/PCL system. This topography is similar to that observed by FESEM, i.e. immiscible PCL-rich domains can be clearly distinguished dispersed in the P3HB matrix. However, the topographic AFM image corresponding to the P3HB/PCL system compatibilized with 1 wt% DCP (**Fig. 7b**) is remarkably different. In fact, no clear evidence of dispersed PCL-rich domains can be seen due to the compatibilization effect provided by reactive extrusion with DCP. This compatibilization leads to lower PCL-rich domain size as well as a more homogeneous PCL-rich domain dispersion. Plot of the elastic modulus image map obtained by the Derjaguin-Muller-Toporov model (**Fig. 7c** and **Fig. 7d**) the microstructure is clearly revealed. A logarithmic plot of the elastic modulus image map reveals some interesting features: (i) the uncompatibilized P3HB/PCL system shows a typical phase-separation morphology in which, spherical PCL-rich domains are uniformly dispersed in the P3HB-rich matrix. Some evidences of interface failure (marked with arrows in **Fig. 7c**) can be observed. Failure occurs because of the lack of cohesion among the interface between the PCL-rich phase and the P3HB-rich phase. This could be related to a pull effect of the ultramicrotome thus supporting the lack (or very low) compatibility between these two polymers. PCL-rich domains possess an average size comprised between 1 and 5 μm. (ii) On the other hand, the morphology of the compatibilized P3HB/PCL system by reactive extrusion with DCP shows a PCL-rich phase finely dispersed in the P3HB-rich phase matrix. PCL-rich phase appears in the form of small filaments with a thickness of less than 1 μm. Although P3HB and PCL are not fully miscible, the effect of the reactive extrusion with DCP is highly positive to achieve somewhat interactions between them. (iii) The typical failure at the PCL-P3HB interface of the uncompatibilized system does not appear in a clear way in the compatibilized blend which confirms improved

interactions among PCL-P3HB interface with the subsequent improvement of mechanical properties at a macro scale. (iv) both elastic modulus image maps are shown under the same scale depth with logarithmic values to show that the contrast between PCL-rich and P3HB rich phases is remarkably lower (the differences in the elastic moduli between phases is much lower) in the compatibilized P3HB/PCL system than the uncompatibilized one. (v) The P3HB-rich phase in the compatibilized blend is darker which is representative for lower elastic modulus values. This effect can be related to a decrease in the overall P3HB crystallinity and/or the formation of P3HB-PCL grafted oligomers and polymer chains. **Fig. 7e** and **Fig. 7f** show the elastic modulus histograms of the uncompatibilized and compatibilized P3HB/PCL systems respectively. Finely dispersed PCL domains possess a narrow distribution centred at 1 GPa for the uncompatibilized P3HB/PCL system, whilst the compatibilized systems offers a distribution centred at ~0.75 GPa. However, the average elastic modulus of the P3HB-rich phase changes from 3.5 GPa (uncompatibilized blend) to 2.7 GPa (DCP compatibilized blend). These results are in total agreement with the previously reported tensile and flexural moduli and similar to previously reported values for this material [50-52]. It is worth to note that the elastic modulus of the P3HB-rich phase was not constant along the whole section, with values varying from 2.5 GPa to 4 GPa. This phenomenon can be explained by taking into account the cooling profile. The highest E value was obtained far from the surface which is related to the higher crystalline character of the P3HB due to lower cooling rates typical of this zone. However, E values of about 2.5 GPa were recorded close to the topmost surface of the sample, probably due to higher amorphous degree of P3HB achieved by higher cooling rates expected in this zone.

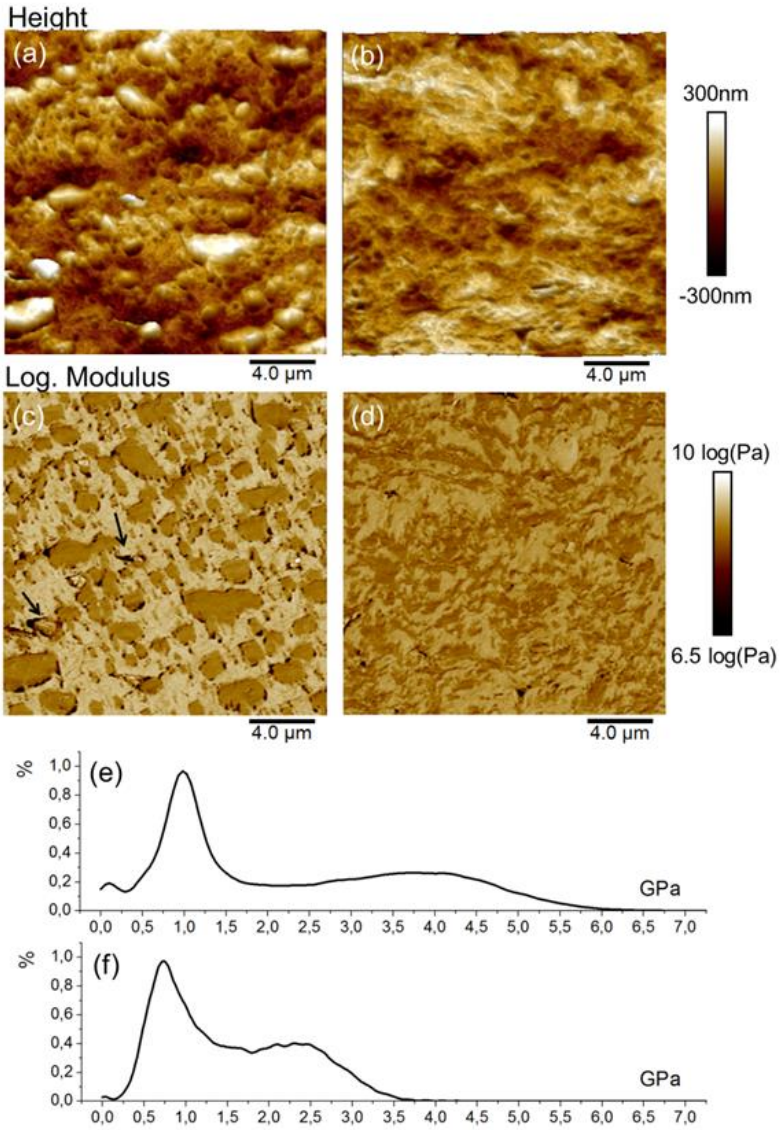

Figure 7. Results obtained by AFM-QNM (20x20 μm^2) showing the topographic AFM image (height channel), the elastic modulus image map (logarithmic scale) and the frequency histogram of the elastic modulus for uncompatibilized P3HB/PCL blend (a, c and e) and DCP compatibilized P3HB/PCL blend (b, d and f)

An in-depth analysis of the elastic modulus image map at higher magnification allowed determining the elastic modulus of each individual phase as observed in **Fig. 8**. The uncompatibilized P3HB/PCL blend (**Fig. 8a** and **Fig. 8c**) shows a stiffness profile characterized by abrupt changes in the elastic modulus value from 2.5-3.0 GPa (P3HB-rich phase) down to 0.75 GPa (PCL-rich phase). On the other hand, the stiffness profile for the DCP compatibilized P3HB/PCL blend is more homogenous as it can be seen in **Fig. 8b** and **Fig. 8d**. The interface width was measured for both uncompatibilized and DCP compatibilized P3HB/PCL blends. Similar values of about 350 nm were observed for both systems thus indicating that compatibilization by reactive extrusion with DCP does not change the mechanical properties profile between the phases but their cohesion. These findings corroborate the hypothesis that reactive extrusion with DCP contributes to improve the interfacial interaction between P3HB-rich and PCL-rich phases, thus leading to a decrease of the elastic modulus of the P3HB-rich phase which seems to be chemically bonded to a PCL-rich phase. All this has a positive effect on mechanical ductile properties with a remarkable increase in the impact-absorbed energy and elongation at break.

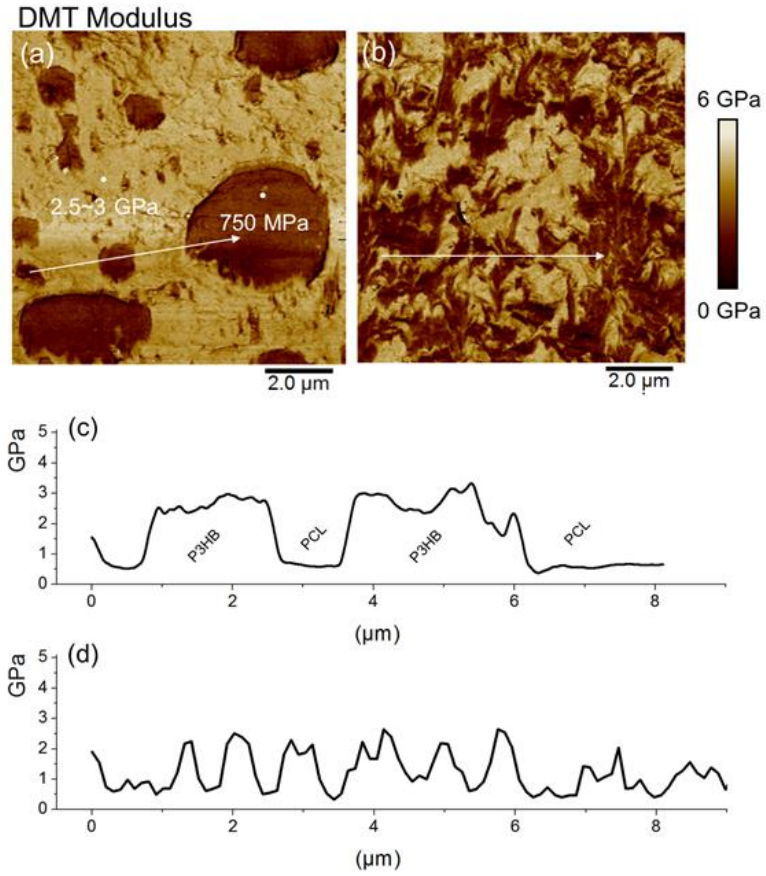

Figure 8. Results obtained by AFM-QNM (10x10 μm^2) the elastic modulus image map and the elastic modulus profile for uncompatibilized P3HB/PCL blend (a and c) and DCP compatibilized P3HB/PCL blend (b and d)

If we take into account the rule of mixtures, the elastic modulus values obtained through the tensile and flexural tests seem to agree to the weighted average values calculated by using the individual elastic modulus values for each phase as obtained by AFM-QNM analysis. As it has been previously stated, the Derjagin-Muller-Toropov (DMT) method was selected to calculation of the elastic modulus versus other proposed models such as Herts, JKR, Oliver & Pharr or Sneddon [53]. The DMT model was selected after an in-depth observation of the force-distance curves taken at different regions which suggested that the adhesion DMT model was more appropriate than the other ones. Fig. 9 shows the force-displacement curve corresponding

to two different AFM indentations on P3HB and PCL. The cantilever translation under a sinusoidal movement of 500 μm amplitude (**Fig. 9a**) generated a clear interaction between the tip and the surface sample in a particular point previously programmed as the Peak Force SetPoint. In this moment, the force-time curve (heart-beat curve) was registered and it is shown in **Fig. 9b** and **Fig. 9c** for the PHB and PCL phase, respectively. Then, the registered signals revealed the typical approximation stage (A) until the electrostatic attraction effect and contact with sample (B) or SetPoint. In this moment, the indentation (B→C stage) occurs, followed by the withdrawal process (C→D). Due to short-range forces and the adhesion effect by capillarity between the sample and the tip, a subsequent stage was revealed. This stage (jump-off-contact) was characterized by a negative force to allow the tip detachment (C→D). The curves obtained for each individual phase show that the necessary force to allow the tip detachment is higher for PCL as it can be seen in the corresponding force-tip sample separation curves (**Fig. 9d** and **Fig. 9e**). The blue represents the trace direction while the red corresponds to the retrace direction. It is clearly deduced that PCL possesses an important adhesive component thus indicating the usefulness of the Derjaguin-Muller-Toporov (DMT) model. On the other hand, this fact reveals that PCL is chemically more active than P3HB. The same picture shows the length used for the DMT adjustment (70% of the unload stage).

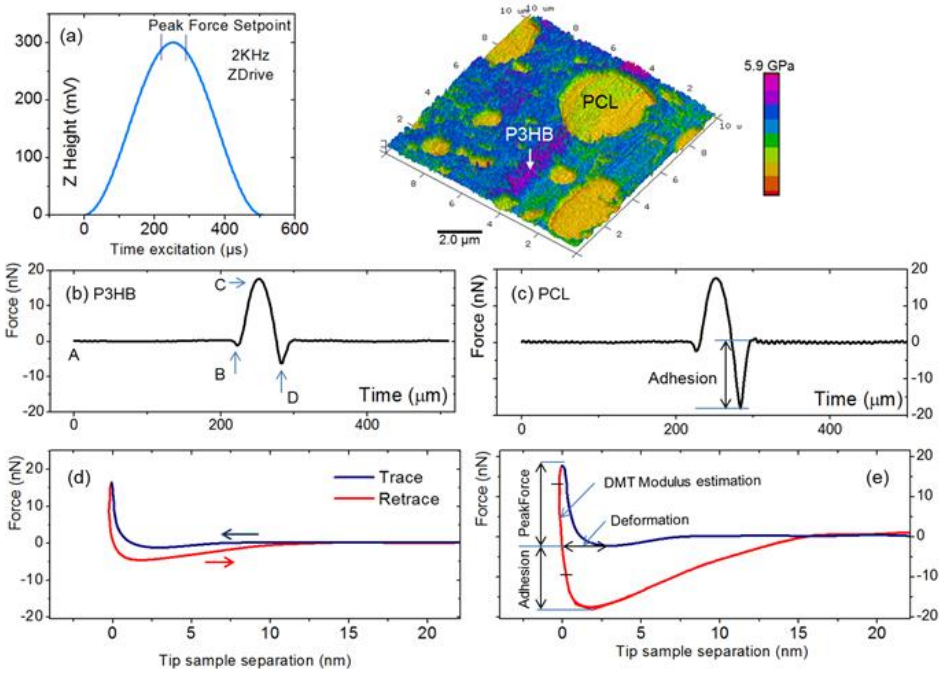

Figure 9. PeakForce curves obtained on P3HB and PCL individual phases, (a) cantilever deflection, (b and c) approach (trace) and withdrawal (retrace) curves, (d and e) force-tip simple separation curves

Fig. 10 shows the deformation and adhesion image maps that are in total agreement with those shown in Fig. 9. The adhesion image maps confirm that PCL offers a higher adhesion component. Furthermore, the DCP compatibilized P3HB/PCL blend shifts the adhesion to higher values as it can be seen in the corresponding adhesion profiles (**Fig. 10d** and **Fig. 10e**). the higher adhesion value observed for the DCP compatibilized P3HB/PCL blend could be related to presence of oxidized moieties resulting from reaction of free radicals achieved during the reactive extrusion with air which leads to a chemically more active surface [49, 54].

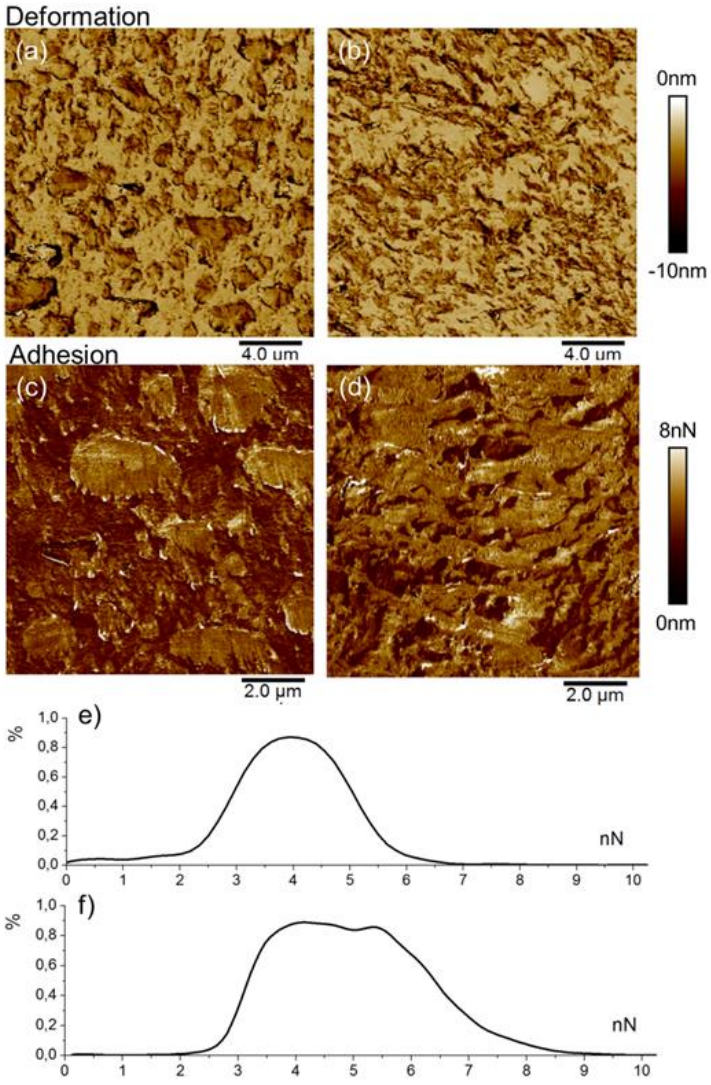

Figure 10. Results obtained by AFM-QNM (10x10 μm^2). Deformation image map (tip penetration), adhesion image map and adhesion profile for uncompatibilized P3HB/PCL blend (a, c and e) and DCP compatibilized P3HB/PCL blend (b, d and f)

Nanomechanical properties

With the aim of obtaining the hardness of the two samples analysed by AFM a 75 indentation array (100 nm depth) was programmed on ultramicrotome samples. The elastic modulus (E) and the hardness values (H) were determined by the well stablished Oliver&pharr

method with some corrections using the Loubet model to correct the adhesion component [44]. It is worth to note that the results obtained by nanoindentation are not comparable to those obtained by AFM as the mathematical models are different and the test depths are also different (100 nm for Nanoindentation and 5-10 nm for AFM). **Fig. 11a** and **Fig. 11b** show the elastic modulus distributions are rather similar to those obtained by AFM analysis. The elastic modulus of the uncompatibilized P3HB/PCL blend shows two different distributions centred at ~4 GPa and at ~2 GPa which correspond to the P3HB-rich phase and the PCL-rich phase respectively (**Fig. 11a**). The average value of the elastic modulus for the uncompatibilized P3HB/PCL blend is 2.5 GPa. With regard to the DCP compatibilized P3HB/PCL blend, it is worth to note that it is difficult to observe the two distributions and the average elastic modulus is around 1 GPa (**Fig. 11b**). These results are in total agreement with those obtained by the AFM technique. Regarding the hardness, it was difficult to observe the different phases but the overall hardness of the uncompatibilized P3HB/PCL blend was remarkably higher (83 MPa) than the DCP compatibilized system with a hardness value of 47 MPa which is in accordance with the previously reported improvement of mechanical ductile properties.

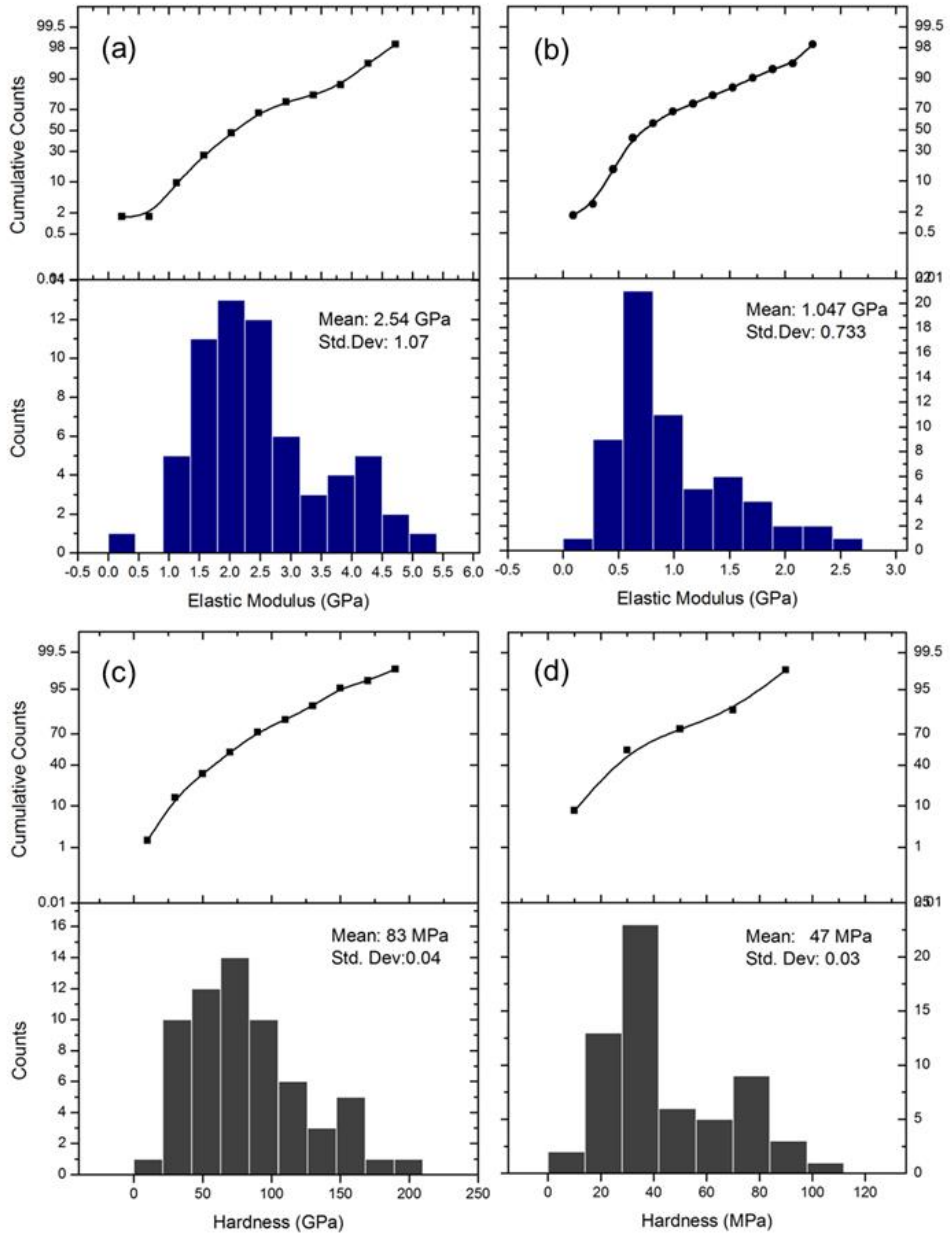

Figure 11. Probability and histogram results of elastic modulus and hardness of uncompatibilized (a,c) and DCP compatibilized P3HB/PCL blend (b,d), obtained by nanoindentation

CONCLUSIONS

The compatibility of binary poly(3-hydroxybutyrate) (P3HB) and poly(ε-caprolactone) (PCL) with a constant composition (75/25 wt/wt) was remarkably improved by reactive extrusion with different dicumyl peroxide (DCP) contents. The use of 1 wt% DCP during *in situ* compatibilization process by reactive extrusion led to a remarkable increase in ductile properties such as elongation at break and impact-absorbed energy with percentage increase of 91% and 231% respectively while the tensile strength remains almost at constant values. FESEM study revealed a clear change in the morphology for *in situ* compatibilized P3HB/PCL (75/25) blend. While the uncompatibilized blend shows a clear phase separation with PCL-rich domains randomly embedded in the P3HB-rich domains, compatibilized blends by reactive extrusion do not show a clear phase separation and the gap between PCL- and P3HB-rich phases has almost disappeared. Results obtained by AFM confirm an increase of compatibility/miscibility between P3HB and PCL by using reactive extrusion with 1 wt% DCP. Although full miscibility is not achieved with DCP compatibilization, the size of PCL-rich domains is remarkably reduced. AFM also revealed a noticeable decrease in the elastic modulus of the P3HB-rich phase thus indicating that some PCL oligomers have been attached to its structure with the subsequent decrease in crystallinity and the corresponding decrease on mechanical resistant properties.

ACKNOWLEDGEMENTS

This research was supported by the Ministry of Economy and Competitiveness – MINECO through the gran number MAT2014-59242-C2-1-R. D. Garcia-Garcia wants to thank the Spanish Ministry of Education, Culture and Sports for the financial support through a FPU grant number FPU13/06011. A. Carbonell-Verdu acknowledges Universitat Politècnica de València for financial support through an FPI grant.

REFERENCES

[1] P. Europe, An analysis of European plastics production, demand and waste data, (2015).

[2] B. Imre, B. Pukánszky, Compatibilization in bio-based and biodegradable polymer blends, 49(6) (2013) 1215-1233.

[3] V. Mittal, T. Akhtar, N. Matsko, Mechanical, thermal, rheological and morphological properties of binary and ternary blends of PLA, TPS and PCL, Macromol. Mater. Eng. 300(4) (2015) 423-435.

[4] M. Arrieta, J. López, D. López, J. Kenny, L. Peponi, Biodegradable electrospun bionanocomposite fibers based on plasticized PLA–PHB blends reinforced with cellulose nanocrystals, (2016).

[5] S.-G. Hong, H.-W. Hsu, M.-T. Ye, Thermal properties and applications of low molecular weight polyhydroxybutyrate, J. Therm. Anal. Calorim. 111(2) (2013) 1243-1250.

[6] C.R. Arza, P. Jannasch, P. Johansson, P. Magnusson, A. Werker, F.H. Maurer, Effect of additives on the melt rheology and thermal degradation of poly [(R)-3-hydroxybutyric acid], J. Appl. Polym. Sci. 132(15) (2015).

[7] M. Auriemma, A. Piscitelli, R. Pasquino, P. Cerruti, M. Malinconico, N. Grizzuti, Blending poly (3-hydroxybutyrate) with tannic acid: Influence of a polyphenolic natural additive on the rheological and thermal behavior, Eur. Polym. J. 63 (2015) 123-131.

[8] P. Mousavioun, W.O. Doherty, G. George, Thermal stability and miscibility of poly (hydroxybutyrate) and soda lignin blends, 32(3) (2010) 656-661.

[9] S. Godbole, S. Gote, M. Latkar, T. Chakrabarti, Preparation and characterization of biodegradable poly-3-hydroxybutyrate–starch blend films, 86(1) (2003) 33-37.

[10] S. Kulkarni, P. Kanekar, S. Nilegaonkar, S. Sarnaik, J. Jog, Production and characterization of a biodegradable poly (hydroxybutyrate-co-hydroxyvalerate)(PHB-co-PHV) copolymer by moderately haloalkalitolerant Halomonas campisalis MCM B-1027 isolated from Lonar Lake, India, 101(24) (2010) 9765-9771.

[11] S. Nakamura, M. Kunioka, Y. Doi, Biosynthesis and characterization of bacterial poly (3-hydroxybutyrate-co-3-hydroxypropionate), 28(S1) (1991) 15-24.

[12] K.J. Ganzeveld, A. van Hagen, M.H. van Agteren, W. de Koning, A.J.S. Uiterkamp, Upgrading of organic waste: production of the copolymer poly-3-hydroxybutyrate-co-valerate by Ralstonia eutrophus with organic waste as sole carbon source, 7(6) (1999) 413-419.

Con formato: Fuente: (Predeterminado) Times New Roman, Inglés (Reino Unido), Revisar la ortografía y la gramática

Con formato: Interlineado: 1,5 líneas

Con formato: Fuente: (Predeterminado) Cambria Math, Inglés (Reino Unido), Revisar la ortografía y la gramática

Con formato: Fuente: (Predeterminado) Times New Roman, Inglés (Reino Unido), Revisar la ortografía y la gramática

Con formato: Fuente: (Predeterminado) Cambria Math, Inglés (Reino Unido), Revisar la ortografía y la gramática

Con formato: Fuente: (Predeterminado) Times New Roman, Inglés (Reino Unido), Revisar la ortografía y la gramática

[13] L. Wang, W. Zhu, X. Wang, X. Chen, G.Q. Chen, K. Xu, Processability modifications of poly (3-hydroxybutyrate) by plasticizing, blending, and stabilizing, J. Appl. Polym. Sci. 107(1) (2008) 166-173.

[14] I. Bibers, V. Tupureina, A. Dzene, M. Kalnins, Improvement of the deformative characteristics of poly-β-hydroxybutyrate by plasticization, 35(4) (1999) 357-364.

[15] D. Garcia-Garcia, J.M. Ferri, N. Montanes, J. Lopez-Martinez, R. Balart, Plasticization effects of epoxidized vegetable oils on mechanical properties of poly (hydroxybutyrate), PHB, Polym. Int. (2016).

[16] C. Hinüber, L. Häussler, R. Vogel, H. Brünig, G. Heinrich, C. Werner, Hollow fibers made from a poly (3-hydroxybutyrate)/poly-ε-caprolactone blend, 5(7) (2011) 643-652.

[17] L. Gunaratne, R. Shanks, Miscibility, melting, and crystallization behavior of poly (hydroxybutyrate) and poly (D, L-lactic acid) blends, 48(9) (2008) 1683-1692.

[18] D. Lovera, L. Márquez, V. Balsamo, A. Taddei, C. Castelli, A.J. Müller, Crystallization, morphology, and enzymatic degradation of polyhydroxybutyrate/polycaprolactone (PHB/PCL) blends, 208(9) (2007) 924-937.

[19] P. Dacko, M. Kowalczuk, H. Janeczek, M. Sobota, Physical properties of the biodegradable polymer compositions containing natural polyesters and their synthetic analogues, Macromolecular symposia, Wiley Online Library, 2006, pp. 209-216.

[20] D. Garcia-Garcia, J.M. Ferri, T. Boronat, J. Lopez-Martinez, R. Balart, Processing and characterization of binary poly(hydroxybutyrate) (PHB) and poly(caprolactone) (PCL) blends with improved impact properties, Polym. Bull. (2016) 1-18.

[21] P. Ma, D.G. Hristova-Bogaerds, P.J. Lemstra, Y. Zhang, S. Wang, Toughening of PHBV/PBS and PHB/PBS Blends via In situ Compatibilization Using Dicumyl Peroxide as a Free-Radical Grafting Initiator, 297(5) (2012) 402-410.

[22] M.F. Díaz, S.E. Barbosa, N.J. Capiati, Reactive compatibilization of PE/PS blends. Effect of copolymer chain length on interfacial adhesion and mechanical behavior, 48(4) (2007) 1058-1065.

[23] L. Yang, J. Huang, X. Lu, S. Jia, H. Zhang, G. Jin, J. Qu, Influences of dicumyl peroxide on morphology and mechanical properties of polypropylene/poly (styrene-b-butadiene-b-styrene) blends via vane-extruder, 132(9) (2015).

[24] W. Michaeli, A. Greefenstein, U. Berghaus, Twin-Screw extruders for reactive extrusion, 35(19) (1995) 1485-1504.

Con formato: Fuente: (Predeterminado) Cambria Math, Inglés (Reino Unido), Revisar la ortografía y la gramática

Con formato: Fuente: (Predeterminado) Times New Roman, Inglés (Reino Unido), Revisar la ortografía y la gramática

Con formato: Fuente: (Predeterminado) Cambria Math, Inglés (Reino Unido), Revisar la ortografía y la gramática

Con formato: Fuente: (Predeterminado) Times New Roman, Inglés (Reino Unido), Revisar la ortografía y la gramática

Con formato: Fuente: (Predeterminado) Cambria Math, Inglés (Reino Unido), Revisar la ortografía y la gramática

Con formato: Fuente: (Predeterminado) Times New Roman, Inglés (Reino Unido), Revisar la ortografía y la gramática

Con formato: Fuente: (Predeterminado) Cambria Math, Inglés (Reino Unido), Revisar la ortografía y la gramática

Con formato: Fuente: (Predeterminado) Times New Roman, Inglés (Reino Unido), Revisar la ortografía y la gramática

Con formato: Fuente: (Predeterminado) Cambria Math, Inglés (Reino Unido), Revisar la ortografía y la gramática

Con formato: Fuente: (Predeterminado) Times New Roman, Inglés (Reino Unido), Revisar la ortografía y la gramática

Con formato: Fuente: (Predeterminado) Cambria Math, Inglés (Reino Unido), Revisar la ortografía y la gramática

Con formato ...

Con formato ...

Con formato ...

Con formato ...

Con formato ...

Con formato ...

Con formato ...

Con formato ...

Con formato ...

Con formato ...

Con formato ...

Con formato ...

Con formato ...

[25] J.M. Raquez, R. Narayan, P. Dubois, Recent Advances in Reactive Extrusion Processing of Biodegradable Polymer-Based Compositions, 293(6) (2008) 447-470.

[26] G. Moad, The synthesis of polyolefin graft copolymers by reactive extrusion, 24(1) (1999) 81-142.

[27] W. Dong, P. Ma, S. Wang, M. Chen, X. Cai, Y. Zhang, Effect of partial crosslinking on morphology and properties of the poly (β-hydroxybutyrate)/poly (d, l-lactic acid) blends, 98(9) (2013) 1549-1555.

[28] R.S. Kurusu, N.R. Demarquette, C. Gauthier, J.M. Chenal, Effect of ageing and annealing on the mechanical behaviour and biodegradability of a poly (3-hydroxybutyrate) and poly (ethylene-co-methyl-acrylate-co-glycidyl-methacrylate) blend, 63(6) (2014) 1085-1093.

[29] M. Arrieta, M. Samper, J. López, A. Jiménez, Combined Effect of Poly(hydroxybutyrate) and Plasticizers on Polylactic acid Properties for Film Intended for Food Packaging, J Polym Environ 22(4) (2014) 460-470.

[30] C.L. Simoes, J.C. Viana, A.M. Cunha, Mechanical Properties of Poly(epsilon-caprolactone) and Poly(lactic acid) Blends, 112(1) (2009) 345-352.

[31] H.-J. Butt, B. Cappella, M. Kappl, Force measurements with the atomic force microscope: Technique, interpretation and applications, 59(1) (2005) 1-152.

[32] S. Frybort, M. Obersriebnig, U. Müller, W. Gindl-Altmutter, J. Konnerth, Variability in surface polarity of wood by means of AFM adhesion force mapping, 457 (2014) 82-87.

[33] G. Smolyakov, C. Formosa-Dague, C. Severac, R. Duval, E. Dague, High speed indentation measures by FV, QI and QNM introduce a new understanding of bionanomechanical experiments, 85 (2016) 8-14.

[34] G. Smolyakov, S. Pruvost, L. Cardoso, B. Alonso, E. Belamie, J. Duchet-Rumeau, AFM PeakForce QNM mode: Evidencing nanometre-scale mechanical properties of chitin-silica hybrid nanocomposites, 151 (2016) 373-380.

[35] J. Roa, G. Oncins, J. Díaz, X. Capdevila, F. Sanz, M. Segarra, Study of the friction, adhesion and mechanical properties of single crystals, ceramics and ceramic coatings by AFM, 31(4) (2011) 429-449.

[36] M.E. Dokukin, I. Sokolov, Quantitative mapping of the elastic modulus of soft materials with HarmoniX and PeakForce QNM AFM modes, 28(46) (2012) 16060-16071.

[37] J. Adamcik, C. Lara, I. Usov, J.S. Jeong, F.S. Ruggeri, G. Dietler, H.A. Lashuel, I.W. Hamley, R. Mezzenga, Measurement of intrinsic properties of amyloid fibrils by the peak force QNM method, 4(15) (2012) 4426-4429.

[38] K. Sweers, K. van der Werf, M. Bennink, V. Subramaniam, Nanomechanical properties of α-synuclein amyloid fibrils: a comparative study by nanoindentation, harmonic force microscopy, and Peakforce QNM, 6(1) (2011) 1.

[39] G. Pletikapić, A. Berquand, T.M. Radić, V. Svetličić, Quantitative Nanomechanical Mapping of Marine Diatom in Seawater Using Peak Force Tapping Atomic Force Microscopy1, 48(1) (2012) 174-185.

[40] B.V. Derjaguin, V.M. Muller, Y.P. Toporov, Effect of contact deformations on the adhesion of particles, 53(2) (1975) 314-326.

[41] W.C. Oliver, G.M. Pharr, Measurement of hardness and elastic modulus by instrumented indentation: Advances in understanding and refinements to methodology, 19(01) (2004) 3-20.

[42] W.C. Oliver, G.M. Pharr, An improved technique for determining hardness and elastic modulus using load and displacement sensing indentation experiments, 7(06) (1992) 1564-1583.

[43] G. Hochstetter, A. Jimenez, J. Loubet, Strain-rate effects on hardness of glassy polymers in the nanoscale range. Comparison between quasi-static and continuous stiffness measurements, 38(5-6) (1999) 681-692.

[44] J. Giró-Paloma, J. Roa, A.M. Díez-Pascual, E. Rayón, A. Flores, M. Martínez, J. Chimenos, A. Fernández, Depth-sensing indentation applied to polymers: A comparison between standard methods of analysis in relation to the nature of the materials, 49(12) (2013) 4047-4053.

[45] P. Ma, X. Cai, Y. Zhang, S. Wang, W. Dong, M. Chen, P. Lemstra, In-situ compatibilization of poly (lactic acid) and poly (butylene adipate-co-terephthalate) blends by using dicumyl peroxide as a free-radical initiator, 102 (2014) 145-151.

[46] T. Semba, K. Kitagawa, U.S. Ishiaku, H. Hamada, The effect of crosslinking on the mechanical properties of polylactic acid/polycaprolactone blends, 101(3) (2006) 1816-1825.

[47] L. Wei, A.G. McDonald, N.M. Stark, Grafting of bacterial polyhydroxybutyrate (PHB) onto cellulose via in situ reactive extrusion with dicumyl peroxide, 16(3) (2015) 1040-1049.

[48] K. Prakalathan, S. Mohanty, S.K. Nayak, Reinforcing effect and isothermal crystallization kinetics of poly(3-hydroxybutyrate) nanocomposites blended with organically modified montmorillonite, Polym. Compos. 35(5) (2014) 999-1012.

[49] D.E. Martínez-Tong, A. Najar, M. Soccio, A. Nogales, N. Bitinis, M. López-Manchado, T. Ezquerra, Quantitative mapping of mechanical properties in polylactic acid/natural rubber/organoclay bionanocomposites as revealed by nanoindentation with atomic force microscopy, 104 (2014) 34-39.

[50] M. Arrieta, J. López, D. López, J. Kenny, L. Peponi, Development of flexible materials based on plasticized electrospun PLA–PHB blends: Structural, thermal, mechanical and disintegration properties, 73 (2015) 433-446.

[51] I. Armentano, E. Fortunati, N. Burgos, F. Dominici, F. Luzi, S. Fiori, A. Jiménez, K. Yoon, J. Ahn, S. Kang, Processing and characterization of plasticized PLA/PHB blends for biodegradable multiphase systems, 9 (2015) 583-596.

[52] M.P. Arrieta, M.a.d.M. Castro-López, E. Rayón, L.F. Barral-Losada, J.M. López-Vilariño, J. López, M.V. González-Rodríguez, Plasticized poly (lactic acid)–poly (hydroxybutyrate)(PLA–PHB) blends incorporated with catechin intended for active food-packaging applications, 62(41) (2014) 10170-10180.

[53] J. J Roa, E. Rayon, M. Morales, M. Segarra, Contact mechanics at nanometric scale using nanoindentation technique for brittle and ductile materials, 6(2) (2012) 116-126.

[54] Å.L. Lyne, V. Wallqvist, B. Birgisson, Adhesive surface characteristics of bitumen binders investigated by atomic force microscopy, 113 (2013) 248-256.

Table captions

Table 1. Composition and labelling of binary poly(3-hydroxybutyrate) (P3HB) and poly(ε-caprolactone) (PCL) blends in situ compatibilized by reactive extrusion with different amounts of dicumyl peroxide (DCP).

Table 2. Thermal parameters of neat P3HB, uncompatibilized P3HB/PCL (75/25) blend and P3HB/PCL (75/25) blends compatibilized by reactive extrusion with different DCP contents

Figure legends

Figure 1. Plot evolution of the gel fraction obtained by soxhlet extraction of the P3HB/PCL (75/25) blend as a function of DCP content used for reactive extrusion

Figure 2. Schematic representation of free radical formation on poly(3-hydroxybutyrate) and poly(ε-caprolactone) polymer chains by reaction with peroxide free radicals

Figure 3. Mechanical properties of the P3HB/PCL (75/25) blend as a function of DCP content used for reactive extrusion: a) tensile properties, b) flexural properties and c) impact properties

Figure 4. DSC curves of the second heating cycle of pure P3HB, uncompatibilized P3HB/PCL (75/25) blend and compatibilized blend by reactive extrusion with different DCP content

Figure 5. Dynamic mechanical thermal analysis (DMTA) of uncompatibilized P3HB/PCL (75/25) blend and compatibilized blends by reactive extrusion with different DCP contents as a function of temperature: a) damping factor, tan δ and b) storage modulus, G'

Figure 6. FESEM images of impact-fractured surfaces of: (a) uncompatibilized P3HB/PCL (75/25) at 2500x; (b) uncompatibilized P3HB/PCL at 5000x; (c) P3HB/PCL (75/25) compatibilized by reactive extrusion with 0.50 wt% DCP at 2500x; (d) P3HB/PCL (75/25) compatibilized by reactive extrusion with 0.50 wt% DCP at 5000x; (e) P3HB/PCL (75/25) compatibilized by reactive extrusion with 1 wt% DCP at 2500x and (f) P3HB/PCL (75/25) compatibilized by reactive extrusion with 1 wt% DCP at 5000x

Figure 7. Results obtained by AFM-QNM (20x20 μm2) showing the topographic AFM image (height channel), the elastic modulus image map (logarithmic scale) and the frequency histogram of the elastic modulus for uncompatibilized P3HB/PCL blend (a, c and e) and DCP compatibilized P3HB/PCL blend (b, d and f)

Figure 8. Results obtained by AFM-QNM (10x10 μm2) the elastic modulus image map and the elastic modulus profile for uncompatibilized P3HB/PCL blend (a and c) and DCP compatibilized P3HB/PCL blend (b and d)

Figure 9. PeakForce curves obtained on P3HB and PCL individual phases, (a) cantilever deflection, (b and c) approach (trace) and withdrawal (retrace) curves, (d and e) force-tip simple separation curves

Figure 10. Results obtained by AFM-QNM (10x10 µm2). Deformation image map (tip penetration), adhesion image map and adhesion profile for uncompatibilized P3HB/PCL blend (a, c and e) and DCP compatibilized P3HB/PCL blend (b, d and f)

Figure 11. Probability and histogram results of elastic modulus and hardness of uncompatibilized (a,c) and DCP compatibilized P3HB/PCL blend (b,d), obtained by nanoindentation